PHYSICAL REVIEW B **75**, 195211 (2007)

Structural and electronic properties of lead chalcogenides from first principles

Kerstin Hummer,* Andreas Grüneis, and Georg Kresse
Department of Computational Materials Physics, Universität Wien, Sensengasse 8/12, A-1090 Wien, Austria

(Received 17 January 2007; published 21 May 2007)

We present *ab initio* calculations on the structural and electronic properties of the narrow-gap lead chalcogenides PbX (X=S, Se, and Te). Particular emphasis is put on the correct description of their exceptional electronic properties compared to III-V and II-VI semiconductors, such as the very small magnitude of the band gap, the unusual order of the band gaps within the series $[E_g(\text{PbS}) > E_g(\text{PbTe}) > E_g(\text{PbSe})]$, and the high effective charge-carrier masses. Within standard density-functional theory (DFT), the local-density approximation (LDA) as well as the generalized gradient approximation (GGA) to the exchange-correlation potential clearly fail to describe important aspects of the band structure of these materials. This problem is overcome by applying methods that go beyond the local or semilocal approximation. We show that hybrid functionals are very successful in giving the correct results for the electronic but also for the structural properties. The lattice constants and bulk moduli as well as the fundamental band gaps and effective masses are in much better agreement with experiment than within DFT-LDA/GGA. The order of the band gaps is also properly obtained. For comparison, partially self-consistent GW_0 calculations are reported, yielding highly accurate values for the band gaps.

DOI: 10.1103/PhysRevB.75.195211 PACS number(s): 71.15.Mb, 71.20.Nr

I. INTRODUCTION

The lead chalcogenides PbX (X=S, Se, and Te) and their alloys represent an attractive class of materials in semiconductor research. Compared to their III-V and II-VI counterparts, these narrow-gap IV-VI semiconductors exhibit unique structural and electronic properties, which make them potential candidates for different technological applications, e.g., thermoelectric, optoelectronic, or spintronic devices. Their importance for long-wavelength sensors, infrared diode lasers, and thermophotovoltaic energy converters[1] has been recognized during the last decades. Furthermore, a technological breakthrough has been recently achieved: the first infrared quantum dot laser based on PbSe/PbEuTe has been realized.[2]

The outstanding properties of these materials motivated a variety of experimental[3,4] as well as theoretical investigations, where the latter comprise calculations on different levels ranging from tight-binding calculations[5] to the empirical pseudopotential method[6,7] and finally to density-functional theory (DFT) methods.[8–10] Compared to the conventional zinc-blende III-V and II-VI semiconductors, the PbX are polar salts that crystallize in the rocksalt structure.[3] Many of their peculiar electronic properties are governed by the interaction of the high lying Pb s electrons that form bands in the valence region with the valence p electrons of the anion X. Due to symmetry, strong *level repulsion* occurs at the L point of the Brillouin zone (BZ), which in turn explains that the fundamental and direct band gap E_g is located at the L point and not at the Γ point as in the III-V and II-VI semiconductors.[8] Besides, the electronic band gap in bulk PbX (X=S, Se, and Te) is very small, ranging from 145 to 286 meV at 4 K (278–410 meV at 300 K) and following the unusual order $E_g(\text{PbS}) > E_g(\text{PbTe}) > E_g(\text{PbSe})$ within the series. Moreover, these materials are characterized by high carrier mobilities (highly anisotropic in the case of PbTe), high dielectric constants, a positive temperature coefficient of the band gaps, as well as a negative pressure dependence of the band gap[3] in contrast to conventional semiconductors.

Concerning the theoretical description, the narrow-gap PbX are interesting and challenging materials. An accurate evaluation of the band structure requires the localized semicore Pb d states to be included as valence states and the inclusion of relativistic effects [spin-orbit coupling (SOC)] for the Pb valence electrons. While standard DFT calculations, i.e., treating the exchange correlation (xc) potential within the local-density approximation (LDA) or generalized gradient approximation (GGA), have been successfully applied to many conventional semiconductors, it turned out that they fail to describe most of the unique electronic properties of the lead chalcogenides. In particular, the band character of the valence-band maximum (VBM) and conduction-band minimum (CBM) is reversed at the L point, resulting in *negative* band gaps, the wrong order of band gaps, and much too low carrier masses. We will show here that a significant improvement can be achieved by methods that go beyond the semilocal approximation, such as hybrid functionals[11,12] or the GW approach.[13]

The main motivation for this work is the *ab initio* investigation of these aspects on the level of standard DFT-GGA as well as by employing hybrid functionals and the GW method. We have performed calculations using the projector augmented wave (PAW) method and the full potential (linearized) augmented plane wave plus local orbital [FP-(L)APW+LO] method. We present a detailed comparison of the results obtained by the different approaches regarding the applied functionals and the underlying basis set (PAW versus APW+LO). Although several DFT LAPW studies of PbX (Refs. 8–10) have been reported previously, we have also performed FP-APW+LO calculations, since different approximations concerning either the treatment of the semicore Pb d states or the SOC have been utilized: in Ref. 8 the underestimation of the LDA band gap was remedied by applying a constant potential to the conduction-band states such that the calculated gaps matched the experimental values and the uncorrected LDA band gap is not stated. Moreover, the calculations were performed using the experimental lattice constants at ambient conditions, whereas the LDA gaps were corrected such that they match the experimental values observed at low temperature. In Ref. 9, the Pb $5d$ states were included as core states in the basis set [the Pb $5d$ band is lacking at around -16 eV in Fig. 1(b) of this reference] and in Ref. 10 spin-orbit effects were treated within the Slater-Koster formalism of tight-binding theory. In the latter approach, the band gaps are adjusted by varying the spin-orbit parameter. In contrast, the results obtained by the PAW and the FP-APW+LO methods presented herein consistently take into account SOC, are parameter-free (except for the approximations involved in the applied density functionals), and incorporate the semicore Pb $5d$ states as valence states.

II. COMPUTATIONAL DETAILS

A. PAW calculations

Most of the results presented in this work have been obtained using the Vienna *ab initio* simulation package (VASP).[14,15] In particular, the PAW method[16,17] has been utilized to construct the basis set for the one-electron wave functions. For standard DFT calculations, the xc energy has been treated within the GGA using the parametrization of Perdew, Burke, and Ernzerhof (PBE).[18] Recently, VASP has been extended to screened hybrid functionals[19] as well as the *GW* method,[20,21] which are employed for a better description of the band gaps. Although there is *per se* no reason to expect a generalized Kohn-Sham scheme to yield good quasiparticle energies, the screened hybrid functional proposed by Heyd *et al.*[22] (HSE03) is performing extremely well for many solids,[23–26] in particular, for band gaps, and thus has been used in this work.

On the DFT level, both the exchange (E_x) and correlation energy (E_c) are treated by an approximation (e.g., LDA or GGA). In contrast, the exchange energy is calculated exactly in the Hartree-Fock (HF) method, whereas the correlation term is usually completely omitted. As a consequence, the HF band gaps of semiconductors are typically significantly too large. On the other hand, the LDA/DFT band gaps are inherently too small due to the lack of the integer discontinuity of the exchange-correlation energy derivative (the well-known *band-gap problem* of DFT).[27] The idea of combining both methods leads to the hybrid functionals. In general, hybrid functionals are constructed by using the DFT correlation energy and adding an exchange energy that consists of 25% Hartree-Fock exchange and 75% DFT exchange. Furthermore, the HSE03 functional proposed by Heyd *et al.*[22] avoids the expensive integrals of the slowly decaying long-ranged part of the Fock exchange by further separating the (E_x) into a short-ranged (SR) and long-ranged (LR) term, where the latter is replaced by its DFT counterpart according to

$$E_{\mathrm{xc}}^{\mathrm{HSE03}} = \frac{1}{4}E_{\mathrm{x}}^{\mathrm{HF,SR}}(\mu) + \frac{3}{4}E_{\mathrm{x}}^{\mathrm{PBE,SR}}(\mu) + E_{\mathrm{x}}^{\mathrm{PBE,LR}}(\mu) + E_{\mathrm{c}}^{\mathrm{PBE}}. \tag{1}$$

In Eq. (1), the additional parameter μ defines the range separation. Nevertheless, the CPU time needed for these HSE03 calculations is by one to two orders of magnitude larger than for standard DFT calculations using (semi)local xc functionals, which strongly depends on the k-mesh representation of the wave function and q-mesh representation of the Fock exchange potential. More details about the implementation of the HSE03 functional in the VASP program can be found in Ref. 19. In the present work, μ was consistently set to $\mu = 0.3\ \text{Å}^{-1} \approx 0.15\ \text{a.u.}^{-1}$ for both the HF and the DFT parts. Strictly speaking, this is not equivalent to the HSE03 implementation of Heyd *et al.*[28]

With respect to the *GW* calculations, it is important to emphasize that the quasiparticle energies have been computed partially self-consistently (GW_0). In the GW_0 approach, based on DFT-PBE wave functions the eigenvalues are updated in the Green's function G until self-consistency is reached, whereas the dielectric matrix of the screened potential W is calculated in the local-density approximation. A recent elaborated study on the *GW* band gaps of various semiconductors and insulators by Shishkin and Kresse has shown that the GW_0 performs better than the commonly utilized single-shot G_0W_0 and also the fully self-consistent *GW* (the eigenvalues are updated in the Green's function as well as the dielectric matrix).[21] They found the trend that the former gives underestimated gaps, whereas the latter yields consistently too large band gaps. Moreover, in the present VASP implementation of the *GW* method, the inclusion of SOC is not possible. Therefore, the effect of SOC on the band gaps has been estimated from HSE03 calculations and subsequently added to the *GW* results.

Except for the evaluation of the effective masses, all band-structure calculations have been performed at the experimental equilibrium lattice constants a at 300 K, which are 5.936, 6.124, and 6.462 Å for PbS, PbSe, and PbTe, respectively. Since the effective carrier masses have been measured at low temperature (roughly 4 K) by Shubnikov–de Haas experiments, these quantities have been calculated using low-temperature lattice constants,[29] which are $a(\text{PbS}) = 5.909$ Å (30 K), $a(\text{PbSe}) = 6.098$ Å (40 K), and $a(\text{PbTe}) = 6.428$ Å (30 K). Since the thermal expansion coefficients below 30–40 K are negligible, it is assumed that the lattice constants at 4 K do not significantly differ from these values.

The parameters for the PAW potentials applied in the present work, i.e., core radii r_c and energy cutoffs E_{cut}, as well as the states treated as valence states are summarized in Table I. The Brillouin-zone integrations have been carried out on Γ-centered k meshes using the tetrahedron method.[30] In the case of DFT-PBE calculations, the equilibrium lattice constants, bulk moduli, and energy gaps have been calculated using $(12\times12\times12)$ grids (corresponding to 72 k points in the irreducible wedge of the BZ), whereas the HSE03 results have been obtained with $(8\times8\times8)$ grids. The core electrons of Pb have been treated fully relativisti-

TABLE I. Core radii r_c and energy cutoffs E_{cut} for the PAW potentials. Non-local projectors were generated for the states listed in the column "Valence." As local PAW-potential a pseudopotential was generated for the states indicated in the column "Local."

	Valence	Local	r_c (a.u.)	E_{cut} (eV)
Pb	$5d^{10}\ 6s^2\ 6p^2$	$5f$	2.5	240
S	$3s^2\ 3p^4$	$3d$	1.9	280
Se	$4s^2\ 4p^4\ 4d^0$	$4f$	2.1	210
Te	$5s^2\ 5p^4\ 5d^0$	$5f$	2.3	175

cally (Dirac equation), whereas the SOC of the Pb valence electrons has been included scalar relativistically.

For evaluating the theoretical lattice constants a_0 and the bulk moduli B_0, the volume dependence of the static lattice energy has been fitted to a Murnaghan equation of state,[31] covering the range Ω/Ω_{eq}=0.9–1.1 with constant steps of 0.01, where Ω_{eq} is the experimental equilibrium volume. In order to avoid effects from the changes in the size of the basis set due to changes in the unit cell volume Ω, the energy cutoff E_{cut} has been increased to 300 eV.

The band structures $E(\mathbf{k})$ have been computed on a discrete k mesh following high-symmetry directions, i.e., from the BZ center Γ with the reciprocal coordinates (0,0,0) to the L point (0.5,0.5,0.5) and W point (0.25,0.5,0.75) in units of ($2\pi/a$, $2\pi/a$, $2\pi/a$). The effective carrier masses $m^*_{\parallel}$ and $m^*_{\perp}$ have been evaluated by fitting the valence band (conduction band) to a parabola according to $E=\frac{\hbar^2k^2}{2m_e m^*_{\parallel,\perp}}$, where m_e denotes the electron rest mass, in a very small range close to L in order to guarantee parabolicity. Note that $m^*_{\parallel}$ corresponds to the direction toward Γ, whereas $m^*_{\perp}$ is perpendicular to $m^*_{\parallel}$ (L toward W).

In the case of the GW_0 calculations, the BZ integrations have been performed on $(8\times8\times8)$ k-point grids using 150 bands for calculating the quasiparticle energies. For more technical details, see Ref. 20.

B. FP-APW+LO calculations

For comparison, we have also applied the FP-APW+LO formalism[32] as implemented in the WIEN2K code[33] to calculate the theoretical lattice constants, bulk moduli, and electronic band gaps of PbX at the GGA level. In order to guarantee equivalence between the PAW and the APW+LO calculations, identical k meshes for the BZ integration and the same xc energy functional (PBE) have been used. The most important WIEN2K specific input parameters R_{MT} and $R_{\mathrm{MT}}K_{\max}$, which determine the accuracy of the calculations, are listed in Table II together with the valence electrons and local orbitals (LOs) used for the wave-function basis sets. In the case of ground-state calculations without SOC, eigenvalues and eigenvectors of the Hamiltonian up to a maximum energy of 2.5 Ry ($E_{\max}$ parameter) have been taken into account for generating the valence charge density expansions. Except for PbS, the largest vector in the Fourier expansion of the charge density ($G_{\max}$) has been set to 14 Ry and the lm combinations, where l (m) denotes the angular momentum (magnetic) quantum number, up to $l_{\max}$=6 have been included for the lattice harmonics expansion. In the case of PbS, the former has been increased to 24 Ry and the latter to 8, respectively.

TABLE II. WIEN2K specific input parameters: the semicore and valence orbitals together with the plane-wave cutoff $R_{\mathrm{MT}}K_{\max}$ and the atomic sphere radii R_{MT} as well as the orbitals for which local orbitals (LOs) have been included in the basis set are listed. An additional Pb $6p_{1/2}$ LO was added for a more accurate treatment of spin-orbit coupling. Note that $K^2_{\max}$ corresponds to the energy cutoff in the PAW calculations.

Solid	Valence	R_{MT} (a.u.)	$R_{\mathrm{MT}}K_{\max}$	LO
Pb	$5d^{10}\ 6s^2\ 6p^2$	2.50	10.0	$5d\ 6s\ (6p)$
S	$3s^2\ 3p^4$	2.50	10.0	$3s$
Se	$3d^{10}\ 4s^2\ 4p^4$	2.50	10.0	$3d\ 4s$
Te	$4d^{10}\ 5s^2\ 5p^4$	2.50	10.0	$4d\ 5s$

Similar as described above for the PAW method, SOC is included fully relativistically for the Pb core electrons and by the second-variation method[34] using scalar relativistic eigenvectors for the valence states. For this procedure, it is necessary to significantly increase $E_{\max}$. Convergence tests with respect to this energy cutoff have proven that an $E_{\max}$ of 9.0 Ry is required for obtaining a converged SOC for the Pb $6p$ states and the energy gap. The present version of WIEN2K also provides an improvement of the spin-orbit basis set by adding a local orbital with a $p_{1/2}$ radial wave function. Thereby, the variational flexibility of the basis set is increased and the dependency of the results on $E_{\max}$ and R_{MT} is significantly reduced.[35] For this reason, we have extended the basis set with a Pb $6p_{1/2}$ LO (the linearization energy of this orbital has been set to a value close to the Fermi energy), which has given converged results using $E_{\max}$ of 4.5 and 5.5 Ry.

As we will see later, the band gaps are strongly influenced by the magnitude of the SOC of the Pb $6p$ states, which is 1.37 eV for the lead atom, as obtained from the solution of the fully relativistic Dirac equation. However, second-variation methods, in particular, without a relativistic LO, are not able to exactly reproduce this value. Therefore, the effect of the chosen basis set and the energy cutoff ($E_{\max}$) on the amount of SOC has been thoroughly analyzed by supercell calculations with a single lead atom in a box using the Γ point only. By analogous PAW supercell calculations, it has been found that a box size of $10\times10\times10$ Å^3 is sufficient to correctly describe the rather extended lead $6p$ wave function. The outcome of these calculations will be discussed together with the band gaps in the following section.

As previously shown by Kuněs *et al.* for face centered cubic (fcc) thorium,[35] the inclusion of an additional Pb $6p_{1/2}$ LO does hardly change the theoretical equilibrium volume, since the SOC in fcc thorium has no major impact on the states involved in the bonding mechanism. This might not be applicable to the lead chalcogenides, since the Pb $6p$ states hybridize with the valence states having mostly anion p character, which is the main bonding mechanism in these materials.[36] Therefore, the volume optimization and calcula-

TABLE III. The theoretical lattice constants a_0 and bulk moduli B_0 calculated using different basis sets (FP-APW+LO and PAW) and xc functionals (GGA-PBE and the hybrid functional HSE03) compared to previously reported values obtained by the FP-LAPW method (Refs. 8 and 9) and experimental data from Refs. 3 and 37. Spin-orbit coupling (SOC) has been included in the theoretical description.

	PbS		PbSe		PbTe	
	a_0 (Å)	B_0 (GPa)	a_0 (Å)	B_0 (GPa)	a_0 (Å)	B_0 (GPa)
Literature						
FP-LAPW PBE[a]			6.232	47.0	6.572	39.4
FP-LAPW GGA[b]	6.012	53.3	6.196	49.1	6.565	41.4
This work						
FP-APW+LO PBE	6.012	52.0	6.226	44.5	6.582	37.5
FP-APW+LO PBE+rel. LO	6.007	50.3	6.221	44.8	6.572	37.6
PAW PBE	6.004	51.2	6.214	44.6	6.568	37.2
PAW HSE03	5.963	55.0	6.170	48.3	6.519	40.4
Experiment (300 K)						
Ref. 37	5.936	62.8	6.124	54.1	6.462	39.8
Ref. 3	5.929	62.2	6.117	54.1	6.443	41.1

[a] Reference 9.

[b] Reference 10.

tion of the elastic properties have been performed using the usual as well as the Pb $6p_{1/2}$ LO extended basis set in the second-variational method for SOC.

III. RESULTS AND DISCUSSION

In the following sections, we discuss the calculated structural, elastic, and electronic (band structures and effective carrier masses) properties of the small-gap lead chalcogenides. Particular emphasis is put on the comparison of standard DFT-PBE results obtained with different basis sets (PAW and FP-APW+LO method) to previously reported calculations. Thereby, it is shown that DFT-PBE is *not able* to accurately describe the electronic properties of these materials and the underlying reasons for that are pointed out. This clearly indicates that methods which go beyond a local approximation are required. By applying the hybrid functional HSE03 or the *GW* method, a significant improvement is achieved and therewith obtained results are in excellent agreement with experimental data.

A. Lattice constants and bulk moduli

In Table III, the calculated lattice constants a_0 and the bulk moduli B_0 of Pb*X* obtained by the different approaches used in the present work are summarized. For comparison, earlier reported results from first-principles calculations[9,10] and experimental data[3,37] are included as well. As expected, the GGA-PBE xc functional overestimates the theoretical lattice constants of the lead chalcogenides, resulting in bulk moduli that are significantly smaller than the experimentally observed ones. This finding applies to both the PAW as well as the FP-APW+LO calculations. The comparison between the two types of FP-APW+LO calculations differing in the treatment of SOC reveals that the extended basis set in the second-variational method very slightly decreases the lattice constants (≈0.1%). The corresponding changes in the bulk moduli are minor. When comparing the present FP-APW+LO results (fifth row in Table III) to earlier reported FP-LAPW lattice constants and bulk moduli,[9,10] the largest observed discrepancies amount to 0.03 Å and 4.6 GPa in PbSe for a_0 and B_0, respectively. These are most likely related to the fact that either the extended Pb $5p$ states were not included in the valence[9] or spin-orbit coupling was treated differently.[10] The previous agreement for the bulk moduli of PbSe and PbTe was clearly fortuitous. We believe that the present results are better converged, as demonstrated by the agreement between the PAW and the FP-APW+LO results.

In fact, the theoretical lattice constants agree within 0.1%, i.e., in the milliangstrom range, whereas for the bulk moduli the largest deviation of approximately 2% is found for PbS. Except in the case of the bulk modulus of PbS, the FP-APW+LO method gives slightly larger numbers than the PAW method for both the lattice constants and the bulk moduli. The excellent agreement between the present FP-APW+LO and the PAW results supports the high accuracy of both our calculations. However, consistently, the lattice constants are overestimated. Thus, the bulk moduli are underestimated compared to experiment when using the gradient corrected functional, i.e., for roughly 20% in the case of PbS and PbSe and ≈8% for PbTe.

The values given in Table III furthermore show that the results obtained by the HSE03 functional are much closer to the experimental findings than those provided by the semilocal functionals. The HSE03 lattice constants are within 1% of the experimental values and the agreement of the bulk moduli is much better, i.e., roughly within 5% in the case of PbS, 10% for PbSe, and 2% for PbTe. The improvement

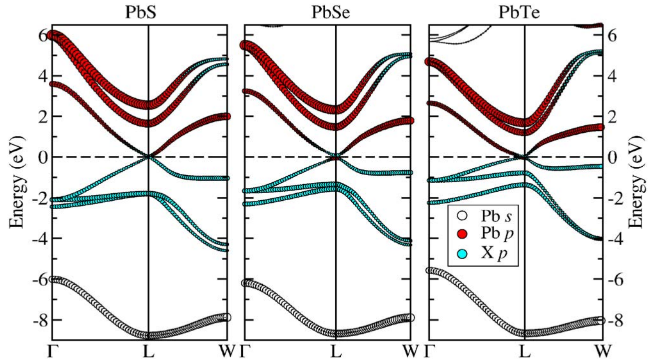

FIG. 1. (Color online) Standard DFT-PBE band structures of PbS, PbSe, and PbTe along ΓLW including SOC. The band character is indicated by circles, where the size correlates with the amount of Pb *s*, Pb *p*, and *X p* characters, respectively. The Fermi level is indicated by the dashed line.

achieved by screened hybrid functionals for the description of structural, elastic, and electronic properties has already been previously pointed out by Heyd *et al.*[24] and recently confirmed by Paier *et al.*[25,26] for a number of conventional semiconductors, metals, as well as insulators. The promising results shown in the present work for the narrow-gap semiconductors Pb*X* are a further indication that hybrid functionals outperform semilocal functionals for semiconducting materials.

B. Band structures

First, we will discuss the main features of the Pb*X* band structures $E(\mathbf{k})$ and the effect of including SOC in the standard DFT-PBE calculations. In Fig. 1, the band structures $E(\mathbf{k})$ are shown along the most important high-symmetry lines in an energy range close to the Fermi level. In contrast to the conventional II-VI and III-V semiconductors, the cation (Pb) 6*s* band is occupied and lies close to the valence bands, which are mainly of anion (*X*) *p* character. This Pb 6*s* band possesses the same symmetry as the highest valence band at the *L* point. Since states with equal symmetry repel each other, this gives rise to strong *level repulsion*, which determines the main features of the band structures and is the origin of their peculiarities, such as (i) the appearance of the direct fundamental band gap at the *L* point resulting from pushing the anion *p* states upward, (ii) the particular order of the band gap within the series $[E_g(\mathrm{PbS}) > E_g(\mathrm{PbTe}) > E_g(\mathrm{PbSe})]$, and (iii) the negative pressure dependence of the band gaps.[3,8] Since the level repulsion is not present at the Γ point, the band gaps there are in the usual order $[E_g(\mathrm{PbS}) > E_g(\mathrm{PbSe}) > E_g(\mathrm{PbTe})]$. In Fig. 1, the most important effect introduced by SOC is also illustrated. Due to SOC of the Pb 6*p* states, which mainly form the conduction bands, one conduction band is lowered in energy at the Γ point. The spin-orbit splitting (SOS) of the Pb 6*p* states at Γ decreases from 2.4 eV in PbS to 2.2 eV in PbSe and 2.0 eV in PbTe. The hybridization between Pb 6*p* and anion *p* states, increasing significantly from PbS to PbTe,[36] also contributes to the SOS of the valence states at Γ, which amounts to 0.3, 0.6, and 1.1 eV for PbS, PbSe, and PbTe, respectively. These values are in excellent agreement with the results of angle-resolved photoemission experiments, i.e., 0.3 eV (PbS), 0.55–0.75 eV (PbSe), and 1.10–1.15 eV (PbTe).[38,39]

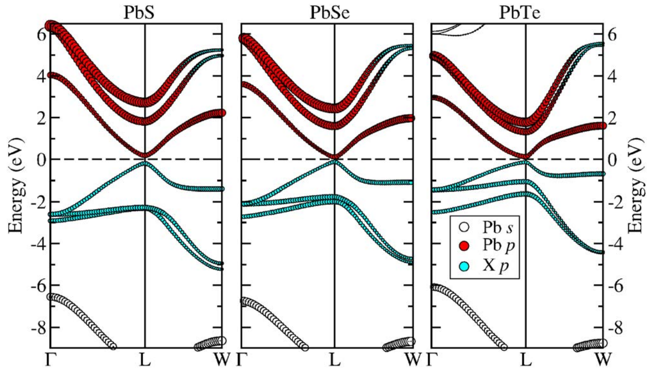

FIG. 2. (Color online) Analogous to Fig. 1: Band structures of Pb*X* calculated using the screened hybrid functional HSE03.

Besides the SOS at the Γ point, there are also significant SOC effects at the *L* point, where the direct energy gap is located. Let us focus on the second and third valence and conduction bands, when going downward and upward from the Fermi level, respectively. Without considering SOC, these bands are degenerated at the *L* point. Due to SOC, this degeneracy is lifted, as evidenced by Fig. 1. Similar to the features observed at the Γ point, the SOS of the conduction-band Pb *p* states decreases within the series from 0.9 eV (PbS), 0.8 eV (PbSe), to 0.5 eV (PbTe). While in PbS, the corresponding SOS of the valence states is negligibly small (0.02 eV), it amounts to 0.2 eV and 0.6 eV in PbSe and PbTe, respectively. However, the main effect on the band structure due to SOC is that the topmost valence band is shifted upward, whereas the lowest conduction band is moved downward in energy, resulting in a significant reduction of the direct energy gap at the *L* point. Even worse, the band character at the *L* point is interchanged such that the valence-band maximum exhibits Pb *p* character and the conduction band mainly anion *p* character (see Fig. 1). This means that the conduction band drops below the valence band, giving rise to *negative* band gaps. In previous *ab initio* calculations,[8,9,36] the well-known underestimation of the DFT-LDA/GGA band gaps in Pb*X* has been stressed, but a thorough analysis of the band character at the *L* point has not been undertaken. Therefore, the qualitative failure of semilocal functionals yielding negative band gaps has not been previously recognized.

Concerning this issue, a qualitative improvement is achieved by applying hybrid functionals. The band structures of Pb*X* calculated using the HSE03 functional are depicted in Fig. 2. Hybrid functionals have already been proven to successfully describe the band gaps of a variety of solids,[24] but band structures of extended systems calculated using HSE03 or similar types of hybrid functionals (B3LYP or PBE0) have only been sparsely discussed in the literature.[40–42]

Compared to DFT-PBE, the main features of the band structures are preserved in the HSE03 calculations, i.e., (i) the direct energy gap is located at the *L* point and (ii) the SOS of the valence and conduction bands at Γ as well as the

TABLE IV. The fundamental band gaps E_g (in eV) at the L point obtained using different xc functionals (DFT-PBE and HSE03) as well as by the GW approach compared to previously reported values calculated with the FP-LAPW method (Refs. 8 and 9) and experimental data from Ref. 37. Values computed without taking into account SOC as well as including SOC are listed. The band gaps correspond to room-temperature values and lattice constants unless explicitly quoted. In the last column, the spin-orbit splitting (SOS) of the Pb $6p$ states (in eV) calculated for the lead atom in a supercell is given.

E_g (eV)	xc	PbS	PbSe	PbTe	SOS Pb $6p$
		Literature			
FP-LAPW[a]	PBE		0.295	0.730	
FP-LAPW+SOC[a]	PBE		0.121	0.160	
FP-LAPW[b]	GGA	0.340	0.380	0.737	
FP-LAPW+SOC[b]	GGA	0.187	0.214	0.188	
		This work			
FP-APW+LO	PBE	0.37	0.29	0.73	
FP-APW+LO+SOC	PBE	0.05	−0.07	0.06	1.23
FP-APW+LO+SOC+rel. LO	PBE	−0.07	−0.18	−0.03	1.36
PAW	PBE	0.37	0.30	0.73	
PAW+SOC	PBE	−0.01	−0.12	−0.01	1.30
PAW	HSE03	0.67	0.58	0.98	
PAW+SOC	HSE03	0.31	0.18	0.25	
PAW+SOC at low temp.	HSE03	0.26	0.13	0.20	
PAW+SOC	GW_0	0.45	0.23	0.30	
PAW+SOC at low temp.[c]	GW_0	0.35	0.15	0.24	
		Experiment			
Ref. 37 at 300 K		0.41	0.28	0.31	
Ref. 37 at 4 K		0.29	0.15	0.19	

[a] Reference 9.
[b] Reference 10.
[c] Reference 21.

L point amount roughly to the same values as given previously. The main differences are observed in the details of the band structure. First, compared to the case without SOC, the character of the highest valence and lowest conduction bands is not interchanged at the L point, resulting in a qualitatively correct band-gap order. Second, the band dispersion of most bands, in particular, of those closest to the Fermi level and of the Pb $6s$ band, is significantly increased. Roughly speaking, it is between 0.1 and 0.4 eV larger, depending on the evaluated direction and material. As we will see later, this enhancement positively affects the effective carrier masses.

C. Fundamental band gaps

The fundamental band gaps of PbX are listed in Table IV. The results of the present work obtained by FP-APW+LO and PAW calculations within standard DFT-PBE without taking into account SOC as well as including SOC, PAW calculations using HSE03, as well as GW calculations on the basis of DFT-PBE wave functions are opposed to previously reported DFT values[9,10] as well as experimental data.[37] For the calculations referred to in Table IV, the experimental lattice constants determined at 300 K have been used unless explicitly quoted. For this reason, the theoretical values are compared to the experimental gaps measured at 300 K and not at low temperatures, as it has often been done before.[8–10]

First, we want to discuss the DFT-PBE results of the FP-(L)APW method compared to the PAW method and the changes due to the inclusion of SOC in both methods. Without taking into account SOC, the band gaps of all three compounds perfectly match [PAW, FP-(L)APW] and they agree well with the literature data of Albanesi *et al.*[9] The larger differences between the present FP-APW+LO band gaps and the values obtained by Mehl *et al.* are assumed to originate from a different GGA xc potential that had been used in the latter work. With respect to experiment, standard DFT-PBE largely overestimates the band gap in PbTe, whereas they are in reasonable agreement in the case of PbS and PbSe. As a consequence, the order of the band gaps in the series is not correctly reproduced by semilocal functionals. When SOC is taken into account, the FP-APW+LO method yields a slightly smaller reduction of the band gaps than the PAW method. In order to trace back these differences, we have performed supercell calculations for a single Pb atom in a box and analyzed the SOS of the Pb $6p$ states, which is given in the last column of Table IV. It was found that the

TABLE V. Effective longitudinal ($m_{\|}^{*}$) and transversal ($m_{\perp}^{*}$) masses at the valence-band maximum (VBM) and conduction-band minimum (CBM) in units of the electron rest mass m_e calculated using the HSE03 functional. For comparison, the DFT-PBE results are given for PbSe. Spin-orbit coupling has been included in the calculations. The experimental values are taken from Refs. 4 and 37.

	$\lvert m_{\|}^{*,VBM}/m_e \rvert$	$\lvert m_{\perp}^{*,VBM}/m_e \rvert$	$\lvert m_{\|}^{*,CBM}/m_e \rvert$	$\lvert m_{\perp}^{*,CBM}/m_e \rvert$
		PAW PBE		
PbSe	0.142	0.144	0.126	0.135
		PAW HSE03		
PbS	0.103	0.071	0.096	0.081
PbSe	0.075	0.040	0.070	0.041
PbTe	0.296	0.029	0.223	0.027
		Experiment		
PbS	0.105±0.015	0.075±0.100	0.105±0.015	0.080±0.010
PbSe	0.066±0.005	0.036±0.002	0.069±0.005	0.037±0.002
PbTe	0.255±0.010	0.024±0.005	0.210±0.005	0.021±0.002

SOC, as it is implemented in the PAW method (VASP code), gives a slightly larger SOS of the Pb $6p$ states (1.30 eV) than the corresponding FP-(L)APW implementation (1.23 eV obtained with the WIEN2K code). Both values are below the result of the solution of the relativistic Dirac equation for the Pb atom (1.37 eV). This is inherent to methods that use scalar relativistic wave functions in the basis set. It is assumed that the differences between the two codes are due to the more flexible PAW basis set made up of plane waves in the entire simulation cell even in the vicinity of the atoms. This is also supported by further FP-APW+LO calculations, where the basis set has been extended by a relativistic local orbital (radial wave function of the Pb $6p_{1/2}$ orbital). The latter raises the SOS to 1.36 eV, which is now close to the fully relativistic solution. This increase of roughly 0.1 eV is also reflected in the corresponding values for the FP-APW+LO+rel. LO band gaps, which are now even smaller (more "negative") than the PAW ones. In summary, compared to the best converged DFT results (FP-APW+LO PBE+SOC+rel. LO), PAW is as close as 60 meV in the case of PbS and PbSe and 20 meV for PbTe.

Including SOC worsens the agreement between theory and experiment in both the PAW and the FP-APW+LO methods. As already pointed out in the last section on the band structures, the calculated band gaps are negative due to the change of the band character of the valence-band maximum and conduction-band minimum at the L point. This had not been found in previously reported FP-LAPW (Refs. 9 and 10) studies, which we believe is either due to the missing Pb $5d$ semicore states in the valence basis set, differences in the treatment of SOC, or due to differences in input parameters, e.g, muffin-tin radii or energy cutoffs, which are particularly important in calculations using SOC. It is also possible that the band character had not been carefully inspected in Refs. 9 and 10, when evaluating the band gaps of the PbX.

Second, we focus on the results of the methods that go beyond semilocal functionals, which are those obtained by the HSE03 functional and the GW method. Both significantly improve the theoretical findings qualitatively as well as quantitatively. PAW HSE03 calculations including SOC yield band gaps of 0.31, 0.18, and 0.25 eV for PbS, PbSe, and PbTe, respectively, which are not only in reasonable agreement with the experimental values of 0.41, 0.28, and 0.31 eV but also reproduce the correct order of the band gaps within the series. While the HSE03 functional underestimates the band gaps in all three compounds with a maximum deviation of 0.1 eV, the GW_0 values, i.e., 0.45 eV (PbS), 0.23 eV (PbSe), and 0.30 eV (PbTe), are in excellent agreement with the experimental findings.

Third, we concentrate on the temperature dependence of the band gaps. The HSE03 band gaps calculated using the low-temperature lattice constants are 0.26 eV (PbS), 0.13 eV (PbSe), and 0.20 eV (PbTe). These values are in good agreement with the experimental data at 4 K, i.e., 0.29 eV, 0.15 eV, and 0.19 eV for PbS, PbSe, and PbTe, respectively. However, they are only 50 meV smaller than the values obtained from the room-temperature lattice parameters in all three compounds, whereas the differences known from experiment are 0.12 eV (PbS), 0.07 eV (PbSe), and 0.12 eV (PbTe). Thus, the experimentally observed significant reduction of the PbS and PbTe band gaps with temperature is not well reproduced using the HSE03 functional. On the other hand, the low-temperature GW_0 calculations perfectly reproduce the temperature induced band-gap reduction in the case of PbS and PbSe but underestimate it in the case of PbTe.

D. Effective charge-carrier masses

The effective charge-carrier masses were evaluated at the L point from the band dispersions of the VBM and CBM as described in Sec. II A. In Table V, the results obtained by the HSE03 functional including SOC are summarized for both the longitudinal ($m_{\|}^{*}$) and transversal ($m_{\perp}^{*}$) effective electron (indicated by the superscript "CBM") and hole ("VBM") masses. As example, the DFT-PBE results obtained for PbSe are included as well. For comparison, experimental values taken from Refs. 4 and 37 are also listed. Since effective masses are determined at low temperature (usually 4 K) by

Shubnikov–de Haas measurements, the PAW HSE03+SOC calculations have been performed at the low-temperature lattice constants. As a consequence of the interchange of VBM and CBM and the concomitant smaller band dispersions, standard DFT-PBE calculations cannot provide correct effective carrier masses. As exemplarily shown for PbSe in Table V, DFT-PBE significantly overestimates both the longitudinal as well as the transversal effective masses. Moreover, the large anisotropy between the longitudinal and transversal carrier masses characteristic for the narrow-gap Pb*X* is not found in the DFT-PBE calculation. In contrast, the HSE03 functional (i) provides absolute values of the longitudinal and transversal effective electron and hole masses that are in excellent agreement with the experimental findings for all three materials under investigation, (ii) consistently yields longitudinal masses that are larger than the transversal ones in all Pb*X*, and (iii) reproduces the anisotropy between the longitudinal and transversal carrier masses, which is most pronounced in PbTe, where it amounts roughly to a factor 10.

IV. CONCLUSIONS

In this work, we have presented both FP-APW+LO and PAW calculations of the structural and electronic properties of narrow-gap lead chalcogenides using the standard DFT-PBE functional, as well as the screened hybrid functional HSE03 and the *GW* method. The DFT-PBE results of both methods are very close, e.g., 0.1% for the lattice constants and 10 meV for the band gaps (if SOC is not included), demonstrating that well converged PAW and FP-(L)APW calculations yield practically the same technical accuracy within the limits established by the applied density functionals. However, local and semilocal functionals (GGA as well as LDA, not shown here) are not able to correctly describe the details of the band structure of these materials, in particular, if spin-orbit coupling is included. As a consequence, (i) the band gaps are severely underestimated leading to negative band gaps due to an inversion of the band character of the valence-band maximum and conduction-band minimum at the *L* point, and (ii) the effective charge-carrier masses cannot be correctly estimated from the band structure. Furthermore, the DFT-PBE lattice constants are overestimated compared to experiment, resulting in significantly underestimated bulk moduli.

A significant improvement of the theoretically predicted properties of Pb*X* is achieved by applying the screened hybrid functional HSE03. The HSE03 lattice constants are only slightly larger than the experimental values and the Pb*X* bulk moduli agree within 5% in the case of PbS, 10% for PbSe, and 2% for PbTe with experiment. Regarding the band gaps, the HSE03 functional yields values in good agreement with experiment, in particular, the order of gaps within the series is correctly reproduced. The band gaps are underestimated by 0.06 eV in PbTe and by 0.1 eV in PbS and PbSe. The best results are achieved by the partially self-consistent GW_0 method, which yields band gaps of 0.45, 0.23, and 0.30 eV for PbS, PbSe, and PbTe, respectively.

The perfect agreement of the calculated longitudinal and transversal effective carrier masses with measured data is also an indication for the success of the HSE03 functional in describing the electronic properties of the lead chalcogenides. This gives motivation to further *ab initio* investigations of the pressure dependence of the band gaps (deformation potentials) and band offsets for the interfaces between Pb*X* materials, as well as the dielectric constants, which will be the subject of future work.

ACKNOWLEDGMENTS

This work has been supported by the Austrian Fonds zurFörderung der wissenschaftlichen Forschung within the special research program Infrared Optical Nanostructures (IR-ON). We are indebted to G. de Wijs for pointing out the incorrect band order in Pb*X* to us and to G. Springholz for fruitful discussions and providing us with the low-temperature lattice constants of Pb*X*.

---

*Electronic address: kerstin.hummer@univie.ac.at. URL: http://cms.mpi.univie.ac.at/

[1] R. Dalven, *Solid State Physics* (Academic, New York, 1973), Vol. 18.

[2] G. Springholz, T. Schwarzl, W. Heiss, G. Bauer, M. Aigle, H. Pascher, and I. Vavra, Appl. Phys. Lett. **79**, 1225 (2001).

[3] R. Dornhaus, G. Nimtz, and B. Schlicht, *Narrow-Gap Semiconductors* (Springer-Verlag, Berlin, 1985).

[4] H. Pascher and G. Bauer, *Lead Chalcogenides: Physics and Applications* (Taylor & Francis, New York, 2003), Vol. 18.

[5] D. L. Mitchell and R. F. Wallis, Phys. Rev. **151**, 581 (1966).

[6] G. Martinez, M. Schlüter, and M. L. Cohen, Phys. Rev. B **11**, 651 (1975).

[7] M. Schlüter, G. Martinez, and M. L. Cohen, Phys. Rev. B **12**, 650 (1975).

[8] S.-H. Wei and A. Zunger, Phys. Rev. B **55**, 13605 (1997).

[9] E. A. Albanesi, C. M. I. Okoye, C. O. Rodriguez, E. L. Peltzer y Blanca, and A. G. Petukhov, Phys. Rev. B **61**, 16589 (2000).

[10] M. Lach-hab, D. Papaconstantopoulos, and M. J. Mehl, J. Phys. Chem. Solids **63**, 833 (2002).

[11] A. D. Becke, J. Chem. Phys. **98**, 1372 (1993).

[12] J. P. Perdew, M. Ernzerhof, and K. Burke, J. Chem. Phys. **105**, 9982 (1996).

[13] L. Hedin, Phys. Rev. **139**, A796 (1965).

[14] G. Kresse and J. Furthmüller, Comput. Mater. Sci. **6**, 15 (1996).

[15] G. Kresse and J. Furthmüller, Phys. Rev. B **54**, 11169 (1996).

[16] P. E. Blöchl, Phys. Rev. B **50**, 17953 (1994).

[17] G. Kresse and D. Joubert, Phys. Rev. B **59**, 1758 (1999).

[18] J. P. Perdew, K. Burke, and M. Ernzerhof, Phys. Rev. Lett. **77**, 3865 (1996).

[19] J. Paier, R. Hirschl, M. Marsman, and G. Kresse, J. Chem. Phys. **122**, 234102 (2005).

[20] M. Shishkin and G. Kresse, Phys. Rev. B **74**, 035101 (2006).

[21] M. Shishkin and G. Kresse (unpublished).

[22] J. Heyd, G. E. Scuseria, and M. Ernzerhof, J. Chem. Phys. **118**, 8207 (2003).

[23] J. Heyd and G. E. Scuseria, J. Chem. Phys. **121**, 1187 (2004).

[24] J. Heyd, J. Peralta, G. E. Scuseria, and R. L. Martin, J. Chem. Phys. **123**, 174101 (2005).

[25] J. Paier, M. Marsman, K. Hummer, G. Kresse, I. C. Gerber, and J. G. Ángán, J. Chem. Phys. **124**, 154709 (2006).

[26] J. Paier, M. Marsman, K. Hummer, G. Kresse, I. C. Gerber, and J. G. Ángán, J. Chem. Phys. **125**, 249901 (2006).

[27] R. O. Jones and O. Gunnarsson, Rev. Mod. Phys. **61**, 689 (1989).

[28] J. Heyd, G. E. Scuseria, and M. Ernzerhof, J. Chem. Phys. **124**, 219906 (2006).

[29] G. Springholz (private communication).

[30] P. E. Blöchl, O. Jepsen, and O. K. Andersen, Phys. Rev. B **49**, 16223 (1994).

[31] F. F. Murnaghan, Proc. Natl. Acad. Sci. U.S.A. **30**, 244 (1944).

[32] E. Sjöstedt, L. Nordström, and D. J. Singh, Solid State Commun. **114**, 15 (2000).

[33] P. Blaha, K. Schwarz, G. K. H. Madsen, D. Kvasnicka, and J. Luitz, WIEN2K, an augmented plane wave plus local orbitals program for calculating crystal properties, Vienna University of Technology, Austria, 2001 (www.wien2k.at).

[34] D. D. Koelling and B. N. Harmon, J. Phys. C **10**, 3107 (1977).

[35] J. Kuneš, P. Novák, R. Schmid, P. Blaha, and K. Schwarz, Phys. Rev. B **64**, 153102 (2001).

[36] A. Delin, P. Ravindran, O. Eriksson, and J. M. Wills, Int. J. Quantum Chem. **69**, 349 (1998).

[37] *Semiconductors: Group IV Elements, IV-IV and III-IV Compounds*, Landolt-Börnstein, New Series, Group III, Vol. 41, Pt. A, edited by O. Madelung, U. Rössler, and M. Schulz (Springer-Verlag, Berlin, 2005).

[38] V. Hinkel, H. Haak, C. Mariani, L. Sorba, K. Horn, and N. E. Christensen, Phys. Rev. B **40**, 5549 (1989).

[39] T. Grandke, L. Ley, and M. Cardona, Phys. Rev. B **18**, 3847 (1978).

[40] J. Muscat, A. Wander, and N. M. Harrison, Chem. Phys. Lett. **342**, 397 (2001).

[41] V. Barone and G. E. Scuseria, J. Chem. Phys. **121**, 10376 (2004).

[42] X.-B. Feng and N. M. Harrison, Phys. Rev. B **69**, 132502 (2005).